Downscaling GOES Land Surface Temperature for Assessing Heat Wave Health Risks

Yitong Jiang, Peng Fu, and Qihao Weng, *Member, IEEE*

***Abstract*—Recent years have witnessed an emerging concern of the health impact of heat waves. A common approach to investigate heat waves is to resort to the geostationary thermal infrared imagery, such as those from the Geostationary Operational Environmental Satellite (GOES) and Meteosat Second Generation. However, coarse spatial resolutions of geostationary images cannot meet the need of assessing and monitoring heat waves in complex urban settings. To address the spatial and temporal variability of heat waves in urban areas, this letter presented a study of analyzing heat wave risk in Los Angeles, USA, by the synergistic use of GOES land surface temperature (LST), auxiliary geospatial, and census data within the framework of Crichton's Risk Triangle (i.e., hazard, exposure, and vulnerability). Principal component analysis and regression analysis were employed to downscale the original GOES LST imagery from 4 to 1 km. The resultant subhourly 1-km LST data was used to characterize and quantify heat hazard. The census population represented the exposure, while existing health, socioeconomic, and physical environmental conditions were used to describe the vulnerabilities. The risk map of heat wave was computed using the weighted indices of hazard, exposure, and vulnerability. The map was further overlaid with a zip-code data layer to generate statistics. The derived risk map showed that areas with high risk were identified in the central city, part of western LA County, and the desert area, based on a 10-point scale rank.**

***Index Terms*—Geostationary Operational Environmental Satellite (GOES), heat wave, land surface temperature (LST), risk assessment, thermal downscaling, urban areas.**

I. Introduction

URBANIZATION and urban population growth result in the increased vulnerability of cities to environmental hazards [1], such as heat wave. Heat wave hazard has been accused of accounting for heat-related illnesses and deaths [2], [3]. The effect of high temperature on respiratory and cardiovascular death indicated that people with certain preexisting health conditions were more vulnerable in heat wave events [4], [5]. Except for preexisting health conditions, socioeconomic status also correlates with the health risk of heat waves. Excess mortality at home and in retirement institutions was greater than that in hospitals [2]. The mortality of widowed, single, and divorced subjects was greater than that of married people [2]. Therefore, social isolation was found to be a key factor. The lack of mobility also contributes to social isolation. Elderly people in hospitals and residential homes and small children also observe increased risks. Because education attainment correlates with house condition, income, and social status, it is reported that heat-related mortality was higher for those with no education versus some years of education [6]. Given the spatial pattern of urban heat island (UHI), people who live in the inner city are more vulnerable during a heat wave event. Moreover, high population density and large amount of vehicles in the inner city results in the increase of anthropogenic heat discharge. In hot days, thermal insulation and air conditioning are two protection measures from heat wave hazard.

Both UHI and heat waves study urban thermal characteristics, yet with different emphases. The study of UHI focuses on the temperature difference between urban and surrounding areas and the spatiotemporal dynamics of hot spots [7]. The study of heat waves addresses the change of thermal condition in a short period of time, and people's adaptation and mitigation to the environment [8]. In other words, the former is more concerned about long-term climate, while the latter is more concerned about short-term meteorological condition. To monitor the movement of heat waves, both high spatial and temporal air temperature are needed. However, the coverage of existing urban meteorological networks is often insufficient to map air temperature with the spatial details of urban areas. Therefore, an accurate estimation of land surface temperature (LST) at high spatial and temporal resolution from remotely sensed data and using it as a surrogate for air temperature are necessary for the monitoring of heat waves. The sensors on polar orbiting satellites, such as Landsat sensors and the Advanced Spaceborne Thermal Emission and Reflectance Radiometer (ASTER), can provide thermal infrared (TIR) data with relatively high spatial resolution. However, their low temporal resolutions are not sufficient for heat wave monitoring. Although the Moderate-resolution Imaging Spectroradiometer (MODIS) and the Advanced Very High Resolution Radiometer (AVHRR) produce 1–2 images per day for the same area, cloud coverage reduces the usage of the image data and thus increases the time between two image acquisitions. The Geostationary Operational Environmental Satellite (GOES) imager on the geostationary satellite has a much higher frequency of observation which is every 15 min, but with a much coarser spatial resolution of 4 km. Therefore, a common solution for characterizing heat wave characteristics is to downscale GOES images from 4 to 1 km while keeping its temporal resolution.

Thermal downscaling is the technique to derive LSTs at high spatial and/or high temporal resolution [9]. The classical way

Manuscript received December 2, 2014; revised January 13, 2015, February 5, 2015, and March 2, 2015; accepted March 3, 2015.

This paper has supplementary dowloadable material available at http://ieeexplore.ieee.org, provided by the authors.

The authors are with the Center for Urban and Environmental Change, Department of Earth and Environmental Systems, Indiana State University, Terre Haute, IN 47809 USA (e-mail: qweng@indstate.edu).

Color versions of one or more of the figures in this paper are available online at http://ieeexplore.ieee.org.

Digital Object Identifier 10.1109/LGRS.2015.2414897

for this purpose is to utilize the inverse relationship between the normalized difference vegetation index (NDVI) and LST as evident in previous studies [10]. In [11], MODIS TIR data were used as a calibration source for GOES TIR data and blended the two different data streams for yielding half-hourly LSTs at 1 km with the prediction accuracy of 2 K. Due to the complexity of thermal landscapes, a single auxiliary variable is not often sufficient for LST downscaling, particularly in heterogeneous urban areas. Hence, more sophisticated models incorporating LST associated variables need to be developed for the downscaling purpose. Four remote sensing indices were employed as endmembers to estimate the LST of four land cover types, including impervious surface, vegetation, bare soil, and water [12]. In [13], principal component analysis (PCA) was applied to a series of auxiliary data and downscaled the Spinning Enhanced Visible and Infrared Imager (SEVIRI) image to 1 km by regression between LST and higher order principal components in central Europe. To address the spatial and temporal variability issue in the studies of heat waves in urban areas, this letter presented a case study of analyzing heat wave risk in Los Angeles County, USA, by the synergistic use of GOES LST, auxiliary geospatial, and census data within the framework of Crichton's Risk Triangle. First, GOES imagery was downscaled from 4 to 1 km using the method developed in [12]. Then, Crichton's Risk Triangle was used to build the heat wave assessment framework. Next, risk areas were ranked with a 10-point risk scale. The operational potential of such an approach is to monitor the pattern change of heat hazard every 15 min at a 1-km resolution. The 15-min temporal resolution is fine enough to catch the temporal dynamics of the hazard, while the spatial pattern can be linked with census data to provide potential target intervention.

II. Data and Methodology

A. Study Area

Los Angeles (LA) County, California, USA, was chosen as the study area. It suffered an extreme heat hazard during the 2006 North American heat wave. On July 22, 2006, the temperature at Woodland Hills in the City of Los Angeles, reached 119 °F (49 °C), making it the highest recorded temperature in the county. LA County covers the majority of greater Los Angeles, Los Angeles-Long Beach-Santa Ana, which ranked 2 in population of urban agglomeration with more than 10 million inhabitants in 2009 [14]. The study area is located in the coastal zone. The atmospheric flow is complicated by UHI, topographic flow, sea breeze, and marine emissions, and the UHI effect increases the temperature difference between land and sea, which may lead to a deeper penetration of see breezes [14]. Given the large urban agglomerations and possible global change in this area, it is important to examine the city's vulnerability to heat hazard to take effective mitigation measures.

B. Data

Data was divided into two categories: temperature and auxiliary data. The GOES-10 Imager possesses five spectral bands, one visible band at 0.55–0.75 μm and four infrared bands at 3.8–4 μm, 6.5–7 μm, 10.2–11.2 μm, and 11.5–12.5 μm, respectively. The data were downloaded from the National Oceanic and Atmospheric Administration (NOAA) comprehensive large array-data stewardship system (http://www.nsof.class.noaa.gov/saa/products/search?datatype_family=GVAR_IMG). The NOAA Weather and Climate Toolkit was used to export the AREA files to tiff format. AREA files are count data with calibration coefficients. The toolkit uses the calibration information contained in the calibration block of the AREA file and converts the raw counts (10-b precision) to brightness temperatures for the IR channels. Then, GOES LSTs were retrieved using the split-window algorithm and coefficients from [15].

Since LST is strongly influenced by such parameters as solar irradiation, albedo, topography, thermal inertia, and vegetation cover [16], auxiliary data were obtained for downscaling. The auxiliary data related to vegetation included MODIS NDVI and enhanced vegetation index (EVI) data products. Albedo in visible, NIR, and short-wave bands and emissivity in MODIS band 31 and band 32 were also selected. In addition, the Shuttle Radar Topography Mission (SRTM) digital elevation data were used in the downscaling. The percentage of imperviousness data in 2011 was downloaded from the National Land Cover Database and was resampled to a 1-km resolution.

C. Methodology

The downscaling method followed the work in [13]. First, PCA was applied on auxiliary data in a 1-km spatial resolution; second, the highest ranked principal components were upscaled to 4 km; third, the regression between GOES LST and selected components was estimated; and finally, LST was estimated in a 1-km spatial resolution. Interested readers can refer to [13] for further details.

The heat wave risk assessment was conducted based on the Crichton's Risk Triangle concept by Buscail *et al.* [8] and Tomlinson *et al.* [17]. Hazard, exposure, and vulnerability are three components to describe risk. For this letter, the hazard was heat wave event and was measured by LST. Exposure refers to the elements that were exposed in the hazard, and was spatially coincided with the hazard; population from census data was chosen to represent exposure. Vulnerability was measured by the affected exposed elements that were vulnerable in the given hazard. Vulnerable components were categorized into preexisting health conditions, socioeconomic status, and physical environment. The 3-D vulnerability index was combined with the exposure index, each weighted 0.25. Then, the combined vulnerability and exposure index was combined with the hazard index, each weighted 0.5, and formed the heat wave risk index, scored from 1 to 10. The rationale behind the assigned weights is the following: 1) temperature was given greater weight because it was assumed as the most important parameter in the assessment, and 2) exposure and vulnerability were weighted equally according to Buscail *et al.* [8] and Tomlinson *et al.* [17].

The spatial resolution of LST affected the choice of the unit for analysis. When computing the mean LST at the census tract level, 43.7% tracts yielded 0 and 1 K because quite a few census tracts in the downtown area were smaller than 1 km^2. Therefore, Zip Code Tabulation Area 2010 (ZCTA) was chosen

as the unit of analysis in this letter. In this case, it calculated mean values from all pixels that fell within a zone of ZCTA and assigned the value to that zone. For the hazard rank, downscaled LST data were aggregated to ZCTA, and mean temperature was calculated for each ZCTA polygon. Then, the mean LST was reclassified into ten zones of hazard index with 1.5 K of interval.

The exposure index was assigned according to the population in each ZCTA. The ZCTA with no population had no exposure and, consequently, no consideration for the risk. We considered three aspects of vulnerability: preexisting health conditions, socioeconomic status, and physical environmental conditions. All data were collected at the ZCTA level. The data of preexisting health conditions were acquired from the Office of Statewide Health Planning and Development. Cardiovascular, respiratory, renal, and psychiatric conditions, the use of drugs (diuretic, psychotropic, and anticholinergic), bed confinement, and inability were defined as the preexisting conditions according to the previous literatures [2], [5]. ICD-9 codes were used to evaluate the preexisting conditions. If the number of patient in a ZCTA was from 1 to 4, the data need to be masked to "< 5" to protect patient confidentiality. We grouped inpatient and emergency room (ER) data together because, if a patient was seen in the ER and then was hospitalized, the ER record went away and became an inpatient record. We assigned the "< 5" cells zero in the computation since their actual values were unknown.

Socioeconomic status was characterized by social isolation, education attainment, extreme age, population density, and health insurance coverage. Social isolation was defined by the percentage of unemployed, percentage of no vehicles available, percentage of renter-occupied houses, and percentage of 1.51 or more occupants per room (overcrowding). The four variables were combined to form an overall score of social isolation. Population over 25 years and over with less than 9th grade or 9th to 12th grade with no diploma was considered as low education attainment. Population less than 5 years and over 65 years was categorized as the extreme age population. The population density was calculated for each ZCTA. The percentage of no health insurance coverage population in labor force and not in labor force was considered. These variables were weighted equally, and a score was assigned to each component of socioeconomic status. The percentage of old buildings (built before 1960) was used to indicate the physical environmental condition, and a corresponding score was assigned.

III. Results

The three highest order principle components were selected, and they accounted for 71.73%, 17.72%, and 11.22% of the variation, respectively. The regression was performed between GOES LST and the selected principle components. The predicted LST based on the regression had a spatial resolution at 1 km and a temporal resolution at 15 min (see Fig. 1). We validated the predicted LST at 10:30 A.M. with the observed LST from the MODIS product MOD11A1, which passed the study area around 10:30 A.M. The result of validation is shown in Fig. 2. We picked the MODIS pixels whose center points are 0.001 decimal degrees (111 m) or less from our predicted LST for validation.

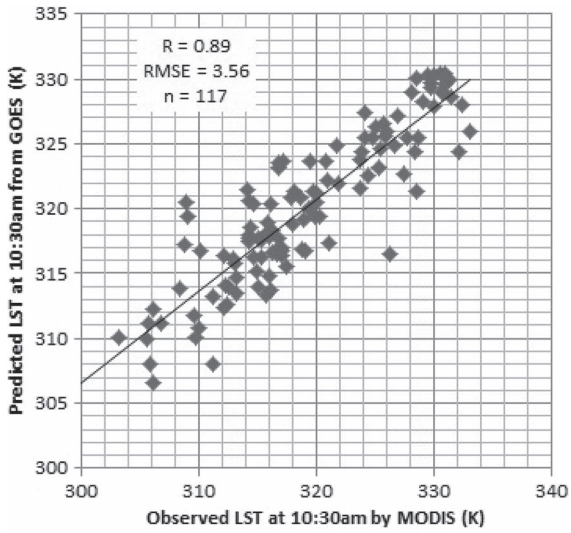

Fig. 1. Validation of the predicted LST from GOES with the observed LST from MODIS. $R = 0.89$, $RMSE = 3.56$, and $n = 117$. The confidence interval at 95% confidence level is 320 ± 1.074, and the margin of error is 1.062.

There are three major benefits of using downscaled high-temporal resolution LSTs to produce a risk index map. First, compared with the original 4-km resolution images, the resultant images showed much more details of temperature variation, particularly in the urban areas, and compared with the MODIS images which are taken twice per day, the resultant images captured the evolvement of UHI and heat waves every 15 min. Second, if we used the daily LST from MODIS, there would be a lot of no-data points due to cloud cover, which further reduced the temporal resolution of the temperature. Since we used interpolation to estimate the no-data points for some of the auxiliary data, the estimated LSTs covered the whole study area. Third, using a hazard index map from different times yielded different risk index maps (see Fig. 3). This proves that the high temporal temperature is necessary in producing the health risk of heat wave events.

According to the selected variables, the risk index map was produced and shown in Fig. 3. The resultant map was categorized into ten classes representing the level of heat wave health risk according to the three major elements: hazard, exposure, and vulnerability indices. Generally, there were three high-risk areas: one at the city center, one at the developed land on the west side of the county, and one in the desert area in the north. To reduce and prevent the heat-related illness and death, these are the areas that the city planner or public health department should work on.

To define a heat wave event, duration (number of hot days), intensity (maximum air temperature), and timing were commonly used [18], [19]. However, since the primary objective was to demonstrate a method that showed changes in the spatiotemporal pattern of heat waves, we only chose 3 h during a hot day, and we used abnormal temperature, i.e., LST greater than 325 K, to define a heat wave event. According to intensity, the northern desert area suffered the highest temperature (see Fig. 2) and was ranked the highest in the hazard index map (see Fig. 3). The exposure in this area was relatively high. The residents were clustered at the intersection of the four ZCTAs.

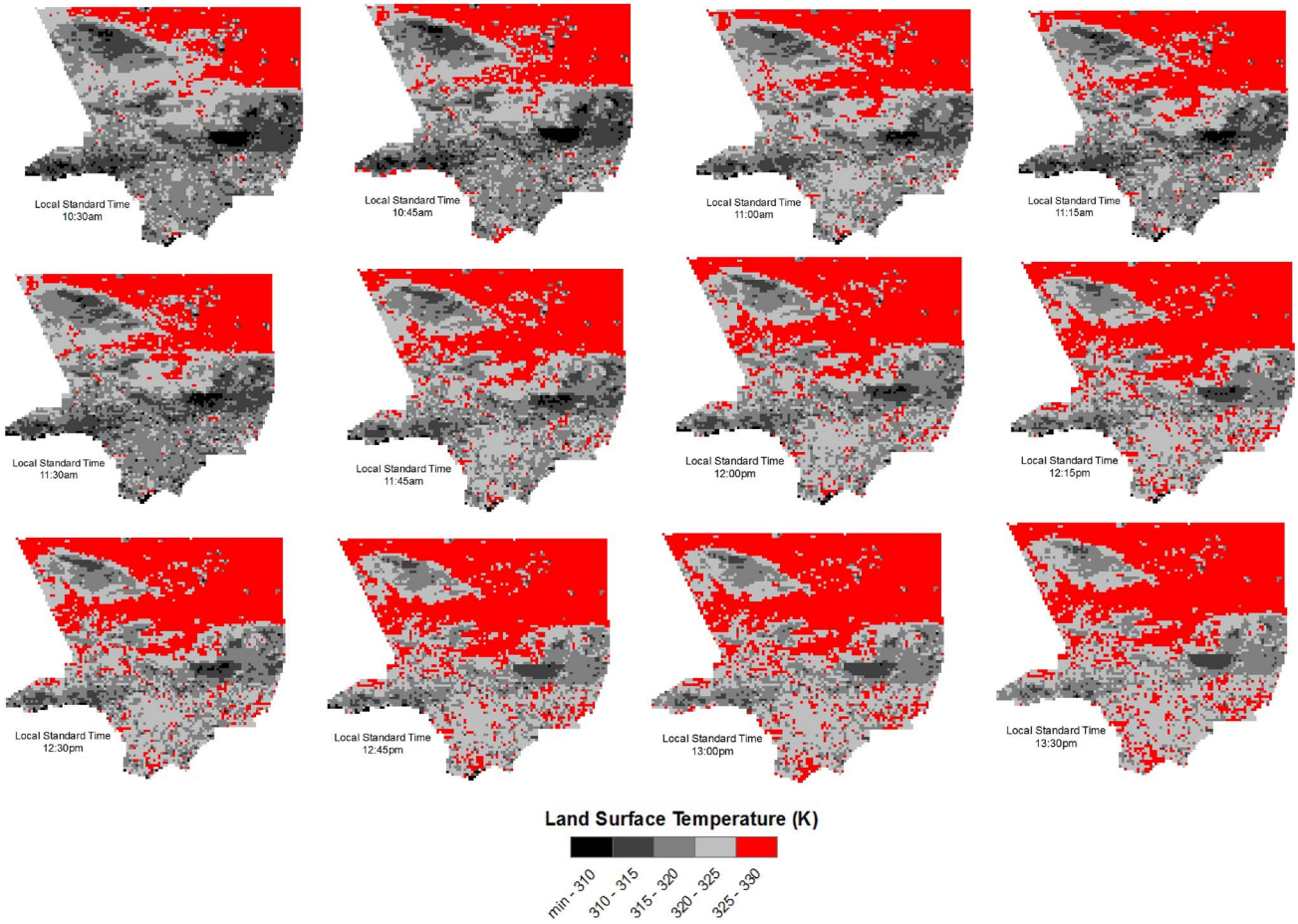

Fig. 2. Spatial and temporal change of LST every 15 min from 10:30 to 13:30, July 18, 2010. This period was chosen because a localized heat wave (with a maximum daily temperature of 31 °C) hit the Los Angeles County at that time, and it lasted for five days from July 14 to July 18. This was four years after the 2010 Northern Hemisphere summer heat waves that struck Los Angeles.

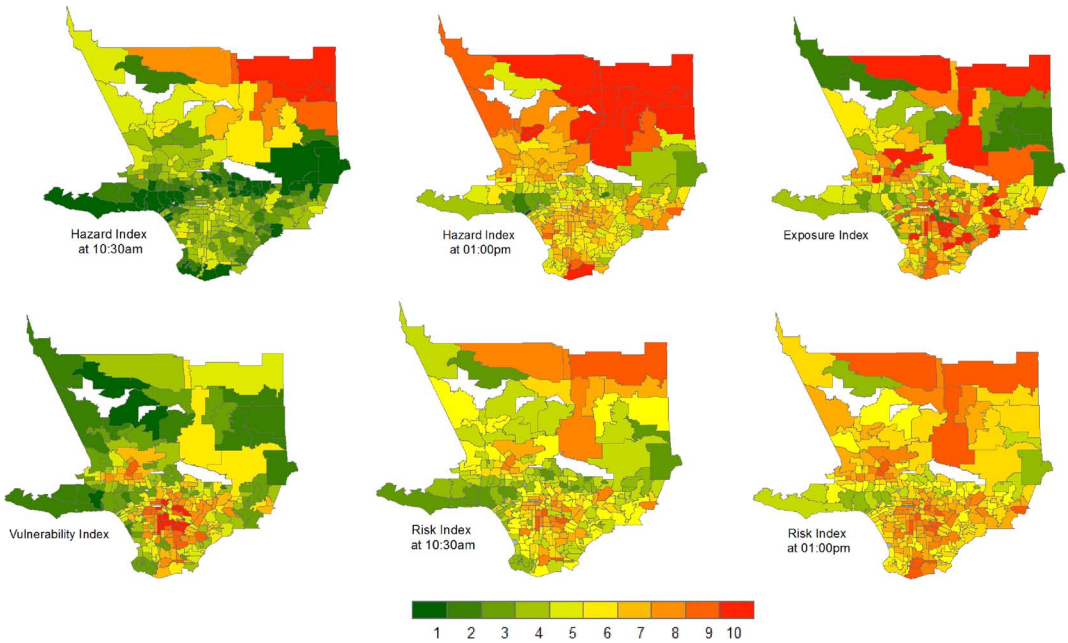

Fig. 3. Hazard indices at 10:30 and 13:00, exposure index, vulnerability index, and risk index generated by hazard, exposure, and vulnerability indices at ZCTA level. The hazard index was produced by the LST at 10:30 and 13:00, respectively, to show the impact of the spatial and temporal variation of LST on heat wave health risk assessment. A supplementary video shows all snapshots and morphing.

This area yielded a low vulnerability index. Therefore, to control hazard and exposure, the key is to reduce the impact of heat wave event in this area. Some agricultural fields were cultivated in the less populated area. Growing plants that adapted to living in an arid habitat might be a way to lower down the LST. Timely and more accurate broadcasting of heat wave event and informing people to stay at the place with air-conditioning may reduce the exposure.

The downtown area in the south was another high-risk area. It experienced high temperature because of the UHI effect. The mountains with high vegetation cover cross the middle of the county and yielded lower surface temperature along the western shoreline. The mountains blocked the onshore breeze from the ocean and strengthened the UHI effect. Different from the northern desert region, the most vulnerable polygons were clustered in this region. Therefore, we selected the four variables of vulnerability index to find a specific way to reduce the vulnerability in the downtown area. In the high-ranked extreme age polygons and high-ranked preexisting condition polygons, we suggest that special care should be provided to children and old people during hot days in the summer. Since excess mortality at home and in retirement institutions was greater than that in hospitals, some hospitals in those areas should be readily available to set up a heat wave-related care section for vulnerable populations during predicted heat wave events. High social isolation polygons were also found in this region. Maybe community engagement programs, public transportation routes, and residential house renovation should be considered in those polygons. For the polygons with high-ranked old buildings, more works need to be done to find out if heat insulation of the buildings should be improved.

The other UHI was located at the western side of the county. The highest exposed ZCTAs were found scattered in the three high-risk areas. The relatively high vulnerable ZCTAs were found in this area as well. Since the vulnerability level was not as high as in the inner city, depending on revenue, less attention may be paid to this area.

IV. Discussion and Conclusion

GOES images were downscaled from 4 to 1 km based on which heat wave health risks were assessed in the Los Angeles County, USA, through the combined weights of hazard, exposure, and vulnerability. The employed downscaling technique increased the spatial resolution and made it possible to examine the characteristics of heat wave hazard at 1 km every 15 min. Moreover, the downscaled results were much more applicable than the original GOES images when overlaying with census data in the risk assessment. The identified high-risk areas suggested possible improvements in allocating revenue and resources and for mitigation strategies. With a 1-km spatial resolution, the suitable unit of analysis was set at the ZCTA level. To better understand the characteristics of heat wave hazard, further study should include air temperature because high air temperature is what people really feel. One problem remain unsolved is how to link LST to air temperature using remote sensing methods. According to the works in [20]–[22], we think that using abnormal LST to represent the general pattern of heat wave is reasonable; however, land cover types, weather, and microclimate conditions associated with urban morphology may create a complex relationship between air and surface temperature.

References

[1] Y. Depietri, T. Welle, and F. G. Renaud, "Social vulnerability assessment of the Cologne urban area (Germany) to heat waves: Links to ecosystem services," *Int. J. Disaster Risk Reduction*, vol. 6, pp. 98–117, Dec. 2013.

[2] A. Fouillet *et al.*, "Excess mortality related to the August 2003 heat wave in France," *Int. Arch. Occup. Environ. Health*, vol. 80, no. 1, pp. 16–24, Oct. 2006.

[3] M. P. Naughton *et al.*, "Heat-related mortality during a 1999 heat wave in Chicago," *Amer. J. Prev. Med.*, vol. 22, no. 4, pp. 221–227, May 2002.

[4] A. L. F. Braga, A. Zanobetti, and J. Schwartz, "The effect of weather on respiratory and cardiovascular deaths in 12 US cities," *Environ. Health Pers.*, vol. 110, no. 9, pp. 859–863, Sep. 2002.

[5] S. Hajat, M. O'Connor, and T. Kosatsky, "Health effects of hot weather: From awareness of risk factors to effective health protection," *Lancet*, vol. 375, no. 9717, pp. 856–863, Mar. 2010.

[6] J. Y. Son, J. T. Lee, G. B. Anderson, and M. L. Bell, "The impact of heat waves on mortality in seven major cities in Korea," *Environ. Health Persp.*, vol. 120, no. 4, pp. 566–571, Apr. 2012.

[7] Q. Weng, "Thermal infrared remote sensing for urban climate and environmental studies: Methods, applications, and trends," *ISPRS J. Photogramm.*, vol. 64, no. 4, pp. 335–344, Jul. 2009.

[8] C. Buscail, E. Upegui, and J.-F. Viel, "Mapping heatwave health risk at the community level for public health action," *Int. J. Health Geogr.*, vol. 11, no. 38, Sep. 2012.

[9] Q. Weng, P. Fu, and F. Gao, "Generating daily land surface temperature at Landsat resolution by fusing Landsat and MODIS data," *Remote Sens. Environ.*, vol. 145, pp. 55–67, Apr. 2014.

[10] W. P. Kustas, J. M. Norman, M. C. Anderson, and A. N. French, "Estimating subpixel surface temperatures and energy fluxes from the vegetation index-radiometric temperature relationship," *Remote Sens. Environ.*, vol. 85, no. 4, pp. 429–440, Jun. 2003.

[11] A. K. Inamdar and A. French, "Disaggregation of GOES land surface temperatures using surface emissivity," *Geophys. Res. Lett.*, vol. 36, no. 2, Jan. 2009, Art. ID. L02408.

[12] G. Yang, R. Pu, C. Zhao, W. Huang, and J. Wang, "Estimation of subpixel land surface temperature using an endmember index based technique: A case examination on ASTER and MODIS temperature products over a heterogeneous area," *Remote Sens. Environ.*, vol. 115, no. 15, pp. 1202–1219, May. 2011.

[13] K. Zaksek and K. Ostir, "Downscaling land surface temperature for urban heat island diurnal cycle analysis," *Remote Sens. Environ.*, vol. 117, pp. 114–124, Feb. 2012.

[14] R. von Glasow *et al.*, "Megacities and large urban agglomerations in the coastal zone: Interactions between atmosphere, land, and marine ecosystems," *Ambio*, vol. 42, no. 1, pp. 13–28. Feb. 2013.

[15] J. Jimenez-Munoz and J. A. Sobrino, "Split-window coefficients for land surface temperature retrieval from low-resolution thermal infrared sensors," *IEEE Geosci. Remote Sens. Lett.*, vol. 5, no. 4, pp. 806–809, Oct. 2008.

[16] Q. Weng, D. Lu, and J. Schubring, "Estimation of land surface temperature-vegetation abundance relationship for urban heat island studies," *Remote Sens. Environ.*, vol. 89, no. 4, pp. 467–483, Feb. 2004.

[17] C. J. Tomlinson, L. Chapman, J. E. Thornes, and C. J. Baker, "Including the urban heat island in spatial heat health risk assessment strategies: A case study for Birmingham, UK," *Int. J. Health Geogr.*, vol. 10, no. 42, Jun. 2011, Art. ID. 3141360.

[18] I. Keramitsoglou *et al.*, "Heat wave hazard classification and risk assessment using artificial intelligence fuzzy logic," *Environ. Monit. Assess.*, vol. 185, no. 10, pp. 8239–8258, 2013.

[19] G. A. Meehl and C. Tebaldi, "More intense, more frequent, and longer lasting heat waves in the 21st Century," *Science*, vol. 305, no. 5686, pp. 994–997, Aug. 2004.

[20] J. Kawashima, T. Ishida, M. Minomura, and T. Miwa, "Relations between surface temperature and air temperature on a local scale during winter nights," *J. Appl. Meteorol.*, vol. 39, no. 9, pp. 1570–1579, Sep. 2000.

[21] N. Schwarz, U. Schlink, U. Franck, and K. Großmann, "Relationship of land surface and air temperatures and its implications for quantifying urban heat island indicators—An application for the city of Leipzig (Germany)," *Ecol. Indicators*, vol. 18, pp. 693–704, Jul. 2012.

[22] K. Callo, R. Hale, D. Tarpley, and Y. Yu. "Evaluation of the relationship between air and land surface temperature under clear- and cloudy-sky conditions," *J. Appl. Meteorol. Climate*, vol. 50, no. 5, pp. 767–775, Mar. 2011.